


Article

Functionalized *Moringa oleifera* Gum as pH-Responsive Nanogel for Doxorubicin Delivery: Synthesis, Kinetic Modelling and In Vitro Cytotoxicity Study

Sunita Ranote^{1,2,3,*}, Marta Musioł¹, Marek Kowalczyk^{1,*} , Veena Joshi², Ghanshyam S. Chauhan³, Rakesh Kumar³, Sandeep Chauhan³ and Kiran Kumar³

¹ Centre of Polymer and Carbon Materials, Polish Academy of Sciences, 34. M. Curie-Skłodowska St., 41-819 Zabrze, Poland

² Department of Chemistry, Hemvati Nandan Bahuguna Garhwal University, SRT Campus, Tehri Garhwal, Srinagar 249199, Uttarakhand, India

³ Department of Chemistry, Himachal Pradesh University, Summer Hill, Shimla 171005, Himachal Pradesh, India

* Correspondence: sranote@cmpw-pan.pl (S.R.); mkowalczyk@cmpw-pan.pl (M.K.); Tel.: +48-734-801-150 (S.R.)

Abstract: Environment-responsive-cum-site-specific delivery of therapeutic drugs into tumor cells is a foremost challenge for chemotherapy. In the present work, *Moringa oleifera* gum-based pH-responsive nanogel (MOGN) was functionalized as a doxorubicin (DOX) carrier. It was synthesized via free radical polymerization through the γ -irradiation method using acrylamide and N,N'-MBA followed by hydrolysis, sonication, and ultracentrifugation. The swelling behavior of MOGN as a function of pH was assessed using a gravimetric method that revealed its superabsorbent nature (365.0 g/g). Furthermore, MOGN showed a very high loading efficiency (98.35 %L) of DOX by MOGN. In vitro release studies revealed that DOX release from DOX-loaded MOGN was 91.92% at pH 5.5 and 12.18% at 7.4 pH, thus favorable to the tumor environment. The drug release from nanogel followed Korsmeyer–Peppas model at pH 5.5 and 6.8 and the Higuchi model at pH 7.4. Later, the efficient DOX release at the tumor site was also investigated by cytotoxicity study using *Rhabdomyosarcoma* cells. Thus, the synthesized nanogel having high drug loading capacity and excellent pH-triggered disintegration and DOX release performance in a simulated tumor environment could be a promising candidate drug delivery system for the targeted and controlled release of anticancer drugs.

Keywords: *Moringa oleifera* gum nanogel; doxorubicin delivery; pH-responsive; release kinetics; *Rhabdosarcoma* cells



Citation: Ranote, S.; Musioł, M.; Kowalczyk, M.; Joshi, V.; Chauhan, G.S.; Kumar, R.; Chauhan, S.; Kumar, K. Functionalized *Moringa oleifera* Gum as pH-Responsive Nanogel for Doxorubicin Delivery: Synthesis, Kinetic Modelling and In Vitro Cytotoxicity Study. *Polymers* **2022**, *14*, 4697. <https://doi.org/10.3390/polym14214697>

Academic Editor: Shih-Jung Liu

Received: 4 October 2022

Accepted: 1 November 2022

Published: 3 November 2022

Publisher's Note: MDPI stays neutral with regard to jurisdictional claims in published maps and institutional affiliations.



Copyright: © 2022 by the authors. Licensee MDPI, Basel, Switzerland. This article is an open access article distributed under the terms and conditions of the Creative Commons Attribution (CC BY) license (<https://creativecommons.org/licenses/by/4.0/>).

1. Introduction

With the advent of newer techniques and treatment methods in the medical world, exponential advancement has been made in cancer biology. Despite the momentous progress in the field of cancer treatment, it is still the foremost cause of death, causing 9.9 million deaths in 2020, out of which around 70% of deaths were reported from developing countries and has proved to be the most noticeable barrier to the long-life expectancy of the human race [1–3]. Several chemotherapeutic drugs have been developed to combat cancer. But their efficacy is limited as most of these drugs have been associated with major shortcomings, viz. poor water solubility and the absence of specificity for cancerous tissues resulting in poor antitumor efficiency, toxicity to the normal tissues, and several side effects such as cardiomyopathy, nephrotoxicity, neurotoxicity, bone marrow suppression and drug resistance [4–6]. Most of these drugs are administered intravenously via injections which results in initial burst release and leads to their consecutive decay; hence, their concentration reaches below the therapeutic level in the blood. Thus, drug specificity is the foremost challenge in the medical field, and it can be overcome by developing efficacious drug-delivery systems with high therapeutic specificity.

Several drug delivery systems have been designed and reported as potential carriers for anticancer drugs, viz. polymeric micelles [7], polypeptides [8], polymeric nanoparticles [9–12], gold nanoparticles [13,14], liposomes [15], silica [16,17], polymersomes [18], nanocomposites [19], nanocapsule [20] and nanogels [21–32]. Among these, stimuli-responsive nanoscale drug delivery systems have attracted researchers' attention worldwide as pH-responsive drug nanocarriers. They have the potential to carry a large amount of drug due to their very high surface/volume ratio and their ability to selectively release the encapsulated drug molecules to the acidic tumor microenvironment either into the lysosomes/late endosomes or escape therefrom to the cytoplasm of the cancer cell [33,34].

For the past few years, a broad range of pH-responsive polysaccharide-based nanocarriers have become the promising subject of research for site-specific anticancer drug delivery as they are cost-effective, biodegradable, biocompatible, non-toxic, and show better compliance with the patient body [26–28,31,35–37]. Moreover, among several nanocarriers, polysaccharide-based nanogels have emerged as the most suitable vehicles for the delivery of anticancer drugs to the targeted site as they possess unique characteristics of large surface area, ease of modification to multifunctional materials, high water adsorption capacity, low interfacial tension with biological fluids and tissues, soft and smooth surface which minimize frictional irritation to the normal tissues [24,34,37,38]. Various studies on designing polysaccharide-based nanogels from various materials, viz. carboxymethyl chitosan, dextrin, chitin, hyaluronic acid, alginate, cellulose, pullulan, and xanthan gum, among others, have been reported in the literature. These nanogels successfully delivered an anthracycline anticancer drug, doxorubicin [22–27,29–33,39,40].

In view of the above-discussed subject matter, a new nanogel was synthesized from plant polysaccharide, *Moringa oleifera* (*M. oleifera*) gum (MOG) using acrylamide (AAm) and *N,N'*-methylenebisacrylamide (*N,N'*-MBA) via γ -irradiation technique followed by partial hydrolysis, sonication, and ultracentrifugation. Later, the synthesized nanogel was evaluated as a carrier for the anticancer drug doxorubicin (DOX). In the present work, keeping in view of the acidic environment of the tumor tissue (pH 6.8 and more acidic in intracellular compartments such as endosomes and lysosomes (5.0–6.5)), acid-sensitive and labile carboxyl groups were introduced via partial hydrolysis of the amide groups of poly(AAm) on *M. oleifera* gum nanogel (MOGN) surface, and these electrostatically interact with the protonated amino groups ($-\text{NH}_3^+$) of DOX [25] to ensure maximum loading and simultaneously ensuring the maximum release of the DOX by its pH-induced swelling behavior. Synthesized nanogel has a very high-water absorption capacity that enables the partitioning of the drug from its solution to the nanogel and results in a high drug-loading capacity. The latter, combined with the pH-responsive nature of the nanogel, renders the reported nanogel an effective carrier and release device of DOX at the tumor site, pH 5.5. In addition, *in vitro* cellular cytotoxicity was also investigated using RD (*Rhabdomyosarcoma*) cells as rhabdomyosarcoma (RMS), a most common soft tissue sarcoma (STS), accounts for over 50% of all the STS detected in teens and children [41]. Moreover, DOX acts as a substrate for ABC transporters present in RD cells, and hence, these cells accrue a substantial amount of DOX chiefly in the lysosomes and nucleus [42]. Thus, the present work highlights the utilization of plant gum, *Moringa oleifera* gum, as an efficient and promising candidate for the targeted delivery of the anticancer drug DOX. To the best of our knowledge, no work related to the synthesis of superabsorbent *M. oleifera* gum nanogel and its application as a pH-responsive delivery of DOX has been reported.

2. Materials and Methods

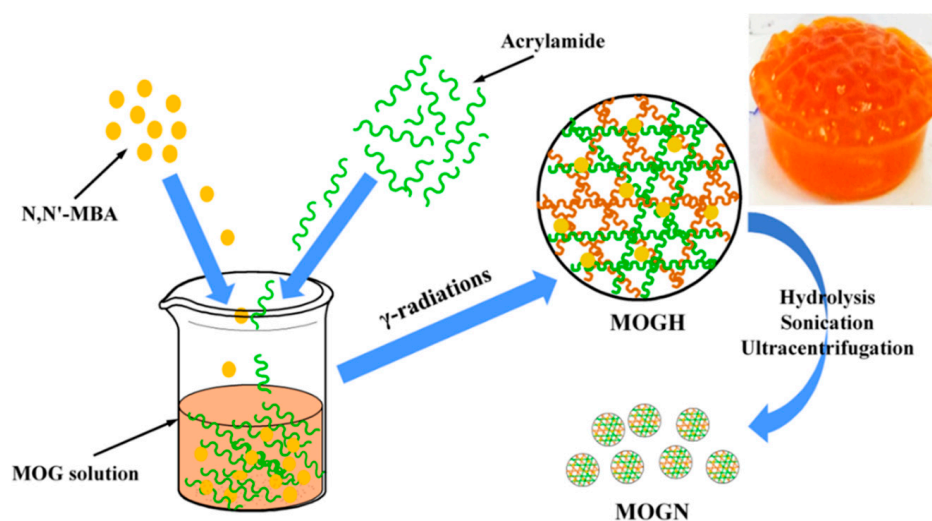
2.1. Reagents and Materials

M. oleifera gum (MOG) was collected from Srinagar, Uttarakhand, India. Doxorubicin hydrochloride (DOX, Samarth Life Sciences Pvt. Ltd., Mumbai, Maharashtra, India), disodium hydrogen orthophosphate anhydrous (Na_2HPO_4), sodium dihydrogen orthophosphate dihydrate ($\text{NaH}_2\text{PO}_4 \cdot 2\text{H}_2\text{O}$), *N,N'*-bismethyleneacrylamide (*N,N'*-MBA), acrylamide (AAm), methanol, hydrochloric acid (HCl), sodium hydroxide (NaOH), dimethyl sulfoxide

(DMSO) (S.D Fine-Chem Ltd., Mumbai, Maharashtra, India), Dulbecco's Modified Eagle's Medium (DMEM), 3-(4,5-dimethylthiazol-2-yl)-2,5-diphenyltetrazolium bromide (MTT), pyridoxal 5'-phosphate (PLP), fetal bovine serum (FBS), penicillin and streptomycin (Hi-Media Lab. Pvt. Ltd., Mumbai, Maharashtra, India) and *Rhabdomyosarcoma* cells (RD cells, National Culture for Cell Science (NCCS), Pune, Maharashtra, India), were of analytical grade. These were used as received. Double distilled water was used in all the experiments.

2.2. Preparation of *Moringa oleifera* Gum Nanogel (MOGN) and DOX-Loaded MOGN (DOX-MOGN)

Purification of crude MOG was performed as per our previously reported work [43]. MOG hydrogel was synthesized via the γ -irradiation method [44]. Briefly, AAm and MOG solution were mixed in a 1:1 weight ratio with constant stirring and then left the mixture undisturbed for 6 h. To the mixture, we added 1% N,N'-MBA (crosslinker) by weight of the mixture components, and it was irradiated in a gamma chamber (^{60}Co -rays) at a dose rate of 0.6 KGy/h for 24 h with a total γ -irradiation dose of 14.4 KGy. After irradiation, the synthesized MOG-hydrogel (MOGH) was equilibrated with distilled water for 72 h to remove any unreacted fractions. Thereafter, MOGH was dried at 50 °C in an oven. To 2.5% solution of MOGH was added 50.0 mL of 2.5 M NaOH to affect its partial hydrolysis, and the contents were stirred for 5 h at 40 °C. Thereafter, 1 N HCl was added under stirring and that was followed by adding acetone for precipitation of the hydrolyzed hydrogel. Finally, the precipitates obtained were washed with 30% methanolic solution and dried at 50 °C in an oven [45]. Later, the hydrolyzed MOGH was converted to nanoform, *Moringa oleifera* gum nanogel (MOGN), by sonication for 24 h at 45 °C followed by ultracentrifugation for 8 h (Scheme 1) [43].



Scheme 1. Synthesis of MOGN (inset image of MOGH).

2.3. Swelling Studies of *Moringa oleifera* Gum Nanogel (MOGN)

The gravimetric method was used to study the swelling behavior of MOGN [44]. For this, 0.01 g of the MOGN was immersed in distilled water, and after a specific time interval, the swollen MOGN was taken out from the solution and wiped with filter paper to remove excess water from its surface. Thereafter, the swollen nanogel was weighed on an electronic weighing balance (Explorer®Analytical and Precision, Ohaus Corporation, New York, NY, USA). The swollen nanogel was dipped into the distilled water again, and the process was repeated until MOGN attained a constant weight. The effect of pH on the swelling behavior of MOGN was investigated using a swelling medium of different pH (2.4, 3.5, 4.5, 5.0, 5.5, 6.8, and 7.4) and distilled water (pH 6.0) in order to mimic the physiological pHs, viz. the

gastrointestinal tract, cancer cells, and interstitial fluid, with time at 37 °C. The swelling ratio (S_r) and %swelling (P_s) was calculated using the following equations [22,24,46]:

$$S_r = \frac{w_s - w_o}{w_o} \quad (1)$$

$$P_s = \frac{w_s - w_o}{w_o} \times 100 \quad (2)$$

where w_s and w_o are the weight of the swollen and dry nanogel, respectively.

2.4. DOX Loading and Release Studies

For the loading of the DOX onto MOGN, 50 mg of MOGN was immersed in 250 mg/L 50 mL DOX solution (prepared in 2% DMSO and phosphate buffer saline solution of pH 7.4) at room temperature. After specific time intervals, the absorbance of the solution containing the residual drug was measured on a UV-Vis spectrophotometer (Photolab 6600) at 495 nm. The amount of the unloaded drug was calculated from a calibration curve. After the optimum drug loading, the DOX-loaded MOGN, i.e., DOX-MOGN, was filtered and washed with distilled water to remove any free drug from its surface. Thereafter, DOX-MOGN was dried at room temperature. The drug loading capacity (q) and loading efficiency (%L) were determined from the expressions [24]:

$$q = \frac{C_o - C_e}{W} \times V \quad (3)$$

$$\%L = \frac{C_o - C_e}{C_o} \times 100 \quad (4)$$

where, C_o is the initial concentration of the drug loaded in time $T = 0$. C_e is the concentration of the drug remaining in the solution (mg/L) in time 't'. V is the volume of the aqueous phase, and W is the amount of dry MOGN.

DOX release studies were carried out in phosphate buffer solutions of pH 5.5, 6.8, and 7.4 to replicate pH values of an intracellular environment of compartments (endosomes and lysosomes), extracellular pH in tumor tissues and the physiological pH in normal tissues, respectively [16,27]. Different drug-loaded samples were separately studied for drug release at the physiological temperature (37 °C) for different time intervals. A known weight of the drug-loaded material was immersed in a specific pH solution, and the amount of released drug was estimated by measuring the absorbance after specific time intervals at 495 nm. %Release (P_r) of the drug was calculated as [26]:

$$P_r = \frac{C_t}{C_o} \times 100 \quad (5)$$

where, C_t is the concentration of the drug released in time 't'. To understand the kinetics and release mechanism of DOX from DOX-MOGN, various kinetic models [47] viz. zero-order [48], first-order [49], Higuchi [50], and the Korsmeyer-Peppas model [51] were applied, and the respective equations are mentioned in Table 1. All the experiments studies were carried out in triplicate, and the results reported are the mean \pm S.D.

Table 1. Various drug-release kinetic models.

| Release Models | Equations | Parameters |
|------------------|--|--|
| Zero-order | $Q_t = Q_0 + k_0 t$ | Q_t = amount of drug released in time 't' Q_0 = initial amount of drug k_0 = zero-order rate constant |
| First-order | $\log Q = \log Q_0 - \frac{k_1 t}{2.303}$ | Q = amount of drug remaining in time 't' k_1 = first-order rate constant |
| Higuchi | $Q_t = k_H t^{1/2}$ | k_H = Higuchi dissolution constant |
| Korsmeyer–Peppas | $\frac{M_t}{M_\infty} = k_{kp} t^n$ or $\log \frac{M_t}{M_\infty} = \log k_{KP} + n \log t$ | M_t/M_∞ = fraction of drug released in time 't' k_{KP} = Korsmeyer–Peppas release rate constant n = drug release exponent |

2.5. Characterization Studies

Synthesized materials were characterized using different techniques to get evidence of MOGN synthesis. Fourier transform infrared (FTIR) spectra of the dry samples were recorded in the transmission mode on a FTIR Spectrophotometer Perkin Elmer Spectrum RX1 (Waltham, MA, USA), between 4000 and 500 cm^{-1} using the KBr pellets under a 300 kgf/cm^2 hydraulic pressure. The surface morphologies of the samples (before and after DOX loading) were observed by field emission scanning electron microscopy (FESEM) images, mapping images, and energy-dispersive X-ray (EDS) spectra and were recorded with Hitachi SU8010 Series FESEM, Tokyo, Japan, at 15 kV. Thermal analysis of the samples was investigated with the TGA/SDTA 851 Mettler-Toledo thermal analyzer from room temperature to 600 °C at a heating rate of 10 °C/min in a stream of nitrogen (60 mL/min). The obtained TGA data were analyzed using the Mettler–Toledo Star System SW 15.00.

2.6. Antitumor Activity Study

2.6.1. Cell Culture

RD cells were cultured in cell culture plates containing DMEM medium with 10% fetal bovine serum (FBS), 1% penicillin, and streptomycin. Thereafter, the cells were incubated for 24 h under a humidified atmosphere at 37 °C with 5% CO_2 atmosphere [52].

2.6.2. Anti-Tumor Activity Assay

The in vitro antitumor activity of free DOX and DOX–MOGN was carried out via MTT assay to determine the viability of RD cancer cell line in the presence of DOX–MOGN using MTT dye which on reduction by mitochondrial dehydrogenase present in living cells forms blue colored formazan crystals [52]. RD cells were suspended in a final concentration of 1.4×10^4 cells/mL in DMEM. This cell suspension was seeded in 96-well plates (200 μL cell suspension/well). The cells seeded in the wells were allowed to grow for 24 h. After incubating, the cells were treated with free DOX and DOX–MOGN at various DOX concentrations (0.01–100 $\mu\text{g/mL}$) for 48 h. Thence, MTT (5 mg/mL in distilled water; 20 μL) was added to each well, followed by incubation at 37 °C in a CO_2 incubator for another 2 h in the dark. Thereafter, the medium was completely removed from each well, and the precipitated intracellular formazan crystals formed in each well were dissolved by adding DMSO (100 μL). After gentle shaking, the absorbance of all the wells was measured at 570 nm with an automated plate reader (Thermo Scientific Multiskan EX Microplate reader, Waltham, MA, USA). Untreated cells were used as the control for 100% cell viability [53]. The treated groups of cells were compared with the control group in the absence of DOX. The half-inhibitory concentration (IC_{50}) was calculated using GraphPad

Prism 7 software. The growth inhibitory ratio, i.e., cell viability (%), was calculated using the following equation [24]:

$$\text{Cell viability (\%)} = \frac{A (\text{Sample})}{A (\text{Control})} \times 100 \quad (6)$$

where A (Control) and A (Sample) are the absorbance values for the untreated cells and treated cells, respectively; these values were obtained after subtracting the absorbance value for DMSO.

The DOX amount calculated by Graph software based on the IC_{50} value was added to the cell culture in a tissue culture flask that contained DMEM low glucose medium (10 mL) marked as a test, and an equal volume of potassium phosphate buffer with PLP was added to the control tissue culture flask. The RD cells with free DOX and DOX–MOGN treatment were examined under the inverted microscope (Inverted Microscope, Hund Wilovert S, Wetzlar, Germany), and images were captured using a camera connected to a laptop with the help of the Software, Magnus Pro 3.0, Olympus. All the assay experiments were carried out in triplicate.

3. Results and Discussion

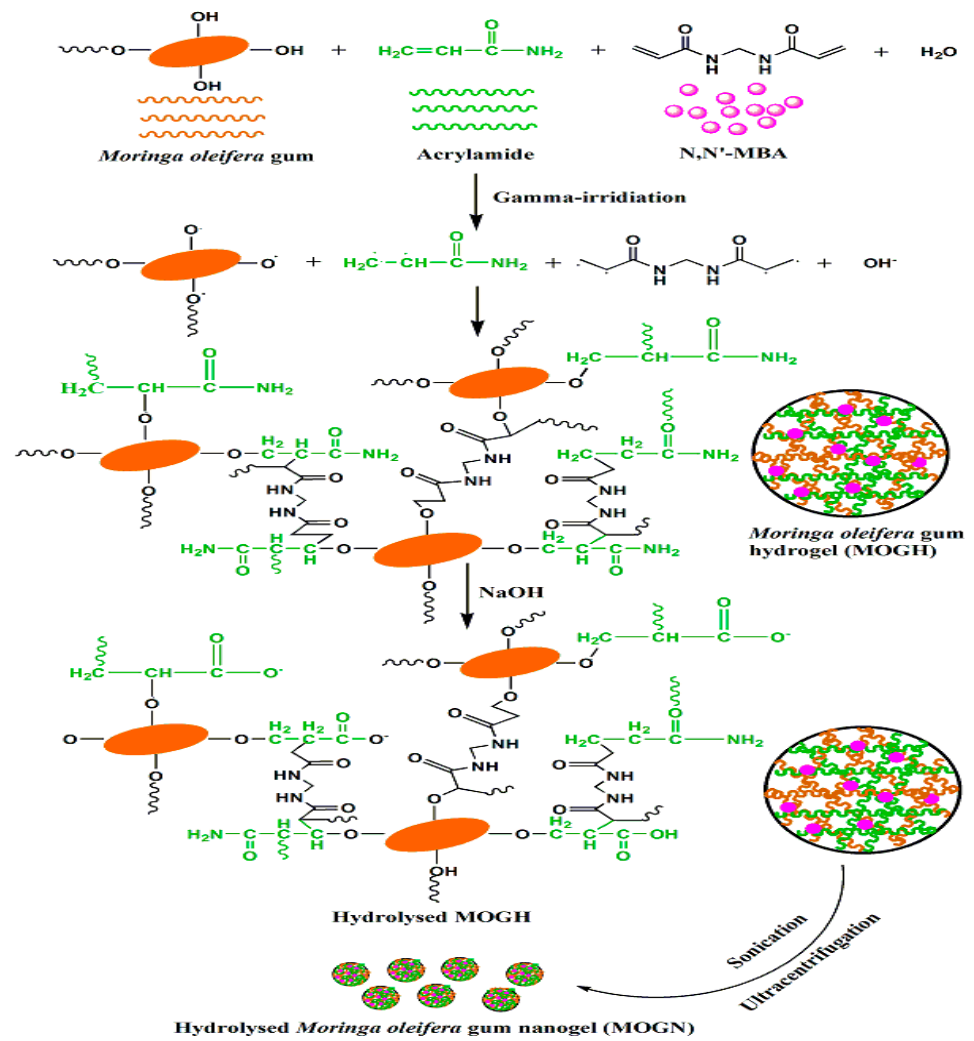
3.1. Synthesis of *Moringa oleifera* Gum Nanogel (MOGN)

Superabsorbent MOGN was synthesized using the γ -irradiation initiation method that involves a free radical mechanism. γ -rays generate free radicals, viz. hydroxyl radical from water and alkoxy radical from MOG, by extracting hydrogen from the –OH groups present in its skeleton. The hydroxyl radicals also abstract hydrogen from the MOG and form an alkoxy radical. These free radicals then attack the vinyl group of acrylamide ($CH_2=CHCONH_2$, AAm) to generate a new radical on the monomer surface that initiates polymerization. Simultaneously, N,N' -MBA reacts with the polymer chain via its vinyl groups by linking with the poly(AAm) and MOG to generate a three-dimensional polymeric network, MOGH. On hydrolysis with NaOH, the – NH_2 groups of MOGH were partially converted into ionized – $COOH$ groups [45]. The hydrolyzed MOGH was converted into nanogel, MOGN, by subjecting it to sonication followed by ultracentrifugation (Scheme 2).

3.2. All Characterization Studies

3.2.1. FTIR Analysis

FTIR spectrum of MOGH has characteristic bands at 3334 cm^{-1} (– $N-H$ stretching vibrations of primary amide), 1657 cm^{-1} (– $C=O$ stretching vibrations of amide II band), 1603 cm^{-1} ($N-H$ bending vibrations), 1421 cm^{-1} ($N-H$ bending vibrations of amide III), 1311 cm^{-1} ($C-N$ stretching vibrations of secondary amide due to the presence of N,N' -MBA) which were absent in pure MOG, along with the characteristic bands of pristine MOG at 1451 cm^{-1} (– COO^- stretching vibrations due to uronic acid of MOG), 1040 cm^{-1} (complex band due to $C-O$ and $C-O-C$ stretching vibrations), and 885 cm^{-1} (pyranose ring modes of polysaccharide skeleton) [45,54]. Whereas, in the FTIR spectrum of MOGN disappearance of the band at 3334 cm^{-1} and 1603 cm^{-1} , along with the appearance of a new band at 1553 cm^{-1} (– COO^- antisymmetric vibrations) and 1405 cm^{-1} (– COO^- symmetric vibrations of ionized – $COOH$ groups) confirms the partial hydrolysis of – NH_2 groups of poly(Aam) [45]. The FTIR spectrum of DOX–MOGN has all the absorption bands of MOGN with a slight change in their position and intensity (Figure 1). Thus, FTIR spectral studies confirm the successful synthesis of MOGN and the loading of DOX on it.



Scheme 2. A plausible mechanism of MOGN synthesis.

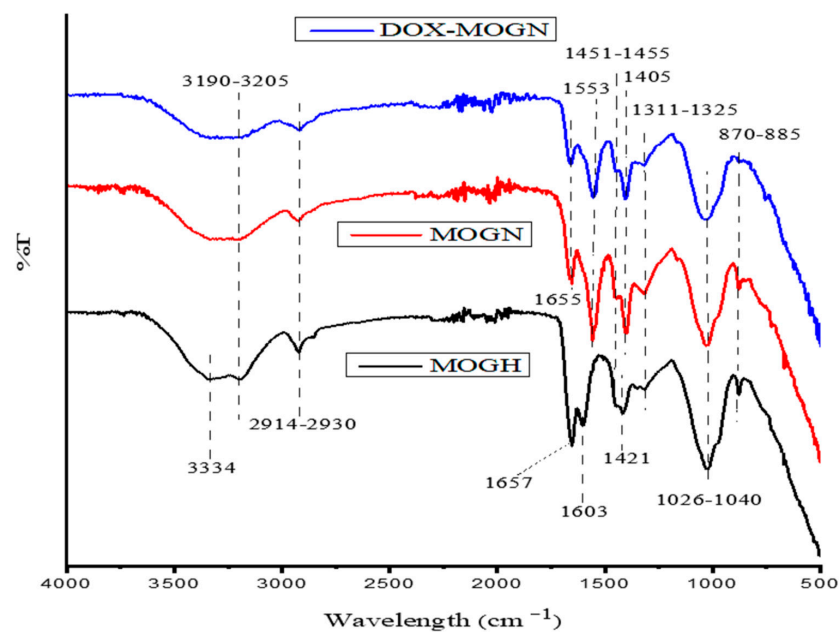


Figure 1. FTIR spectra of MOGH, MOGN, and DOX-MOGN.

3.2.2. SEM Analysis

From the SEM image of MOGN, it can be seen that particles are spherical in shape with a size of <45 nm (Figure 2a), which confirms the nano-dimensional spherical structure of the synthesized nanogel, thus indicating its suitability for drug delivery applications. While the SEM image of DOX–MOGN showed a somewhat rough surface due to the deposition of the drug molecules on its surface (Figure 2b). In addition, the successful loading of DOX onto MOGN was further confirmed by EDS spectra of MOGN and DOX–MOGN.

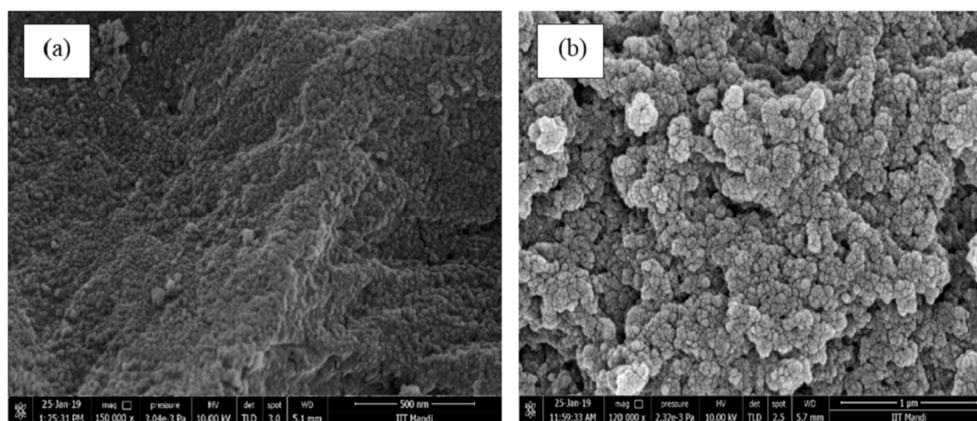


Figure 2. SEM images of MOGN (a) and DOX–MOGN (b).

3.2.3. EDS and Elemental Mapping Analysis

The EDS spectrum of MOGN displayed a new peak of N due to the incorporation of acrylamide and N,N'-MBA along with the characteristic peaks of C and O in the EDS spectrum of MOG [54], indicating its successful synthesis from MOG. Furthermore, a change in the %weight of C, O, and N in the EDS spectrum of DOX–MOGN confirmed the successful loading of DOX onto MOGN (Figure 3a,b). Elemental mapping of MOGN and DOX–MOGN validates the presence of C, O, and N elements and increases the uniform distribution of N in DOX–MOGN than MOGN, confirming the effective loading of DOX onto MOGN (Figure 4a,b).

3.2.4. Thermal Analysis

Thermal analysis of the pure and hydrolyzed grafted form of MOG was investigated using TGA and DTG curves and is depicted in Figure 5a,b. Based on the TGA and DTG curves for pure MOG, two mass loss events were observed wherein the first initial mass loss of 10.9% occurred at >150 °C with a peak at the maximum decomposition temperature (T_{max}) of 65.99 °C due to the evaporation of moisture content and the second major mass loss occurred between 253 °C–400 °C (final decomposition temperature, T_f) are associated with the decomposition of the polysaccharide backbone of MOG. After that, the residual part degraded slowly up to 550 °C, leaving a constant residual mass of 24.4% [55]. In addition, in MOG, a 50% mass loss was observed at 309.68 °C, and this temperature is designated as T_{50} . In the thermogram of the hydrolyzed grafted form, i.e., MOGN, additional multiple mass loss steps were observed. The initial mass loss of 5% due to evaporation of water occurred at >100 °C with T_{max} at 66.21 °C, and second and third mass losses occurred from 140 °C to 200 °C and from 256.74 °C to 392.71 °C with T_{max} at 156 °C and 301.15 °C. They are associated with the degradation of the N,N'-MBA and polyacrylamide chains in the MOGN skeleton, respectively. The fourth mass loss up to 500 °C (final decomposition temperature, T_f) is attributed to the degradation of the remaining polymer backbone. Thereafter, the slow degradation of residual mass was continued till 600 °C [23,56]. In addition, in the thermogram of MOGN, 50% mass loss occurred at 443.32 °C (T_{50}), which was higher than pure MOG. Hence, the T_{50} and T_f were higher for MOGN than its pure form, thus,

indicating that incorporation of polyacrylamide and *N,N'*-MBA enhanced the thermal stability of the synthesized MOGN.

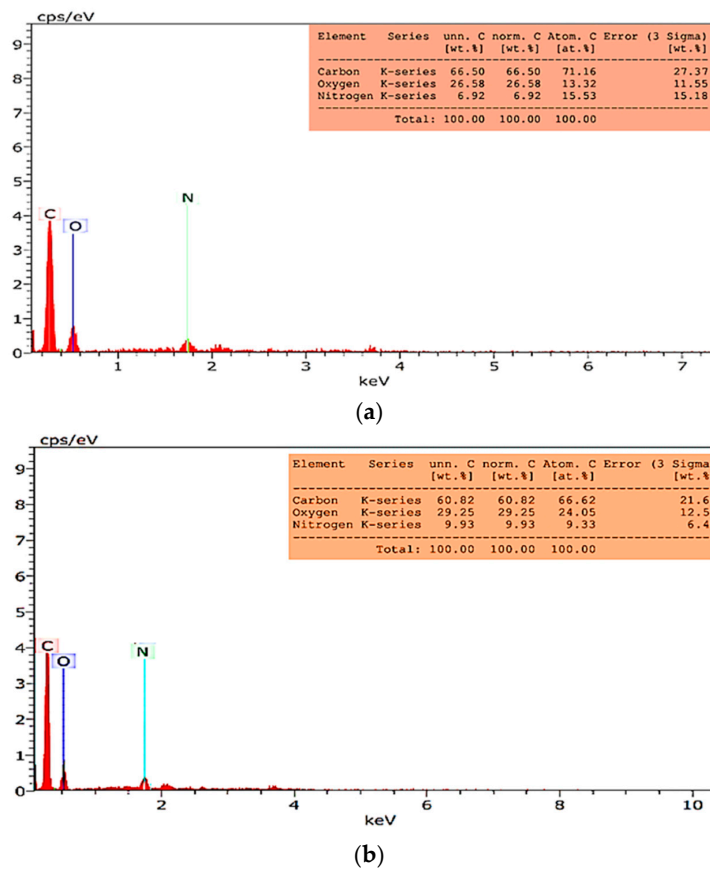


Figure 3. EDS spectra of MOGN (a) and DOX-MOGN (b).

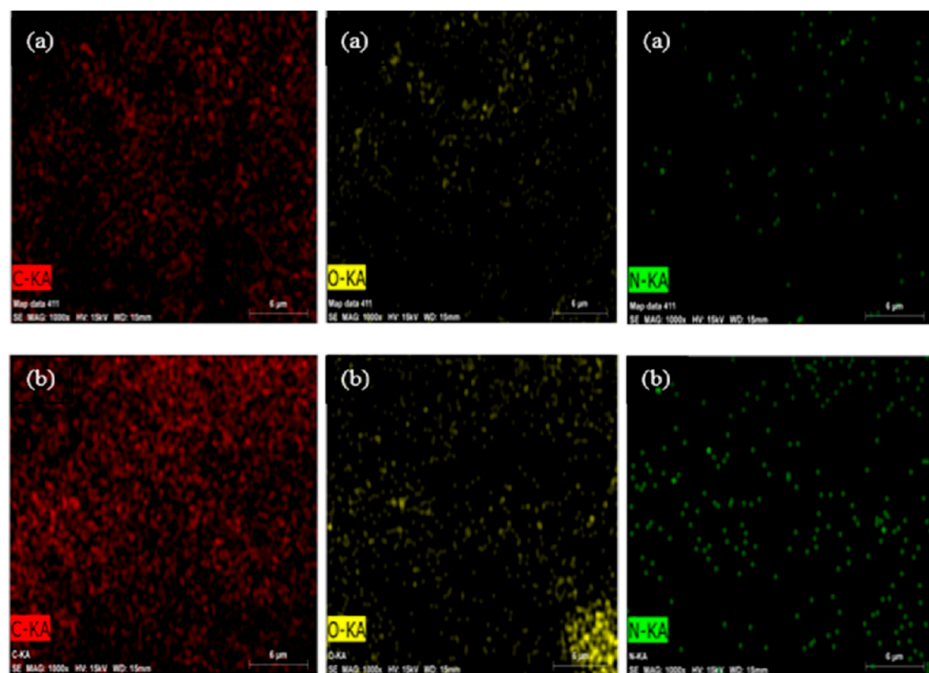


Figure 4. Elemental mapping images of MOGN (a) and DOX-MOGN (b).

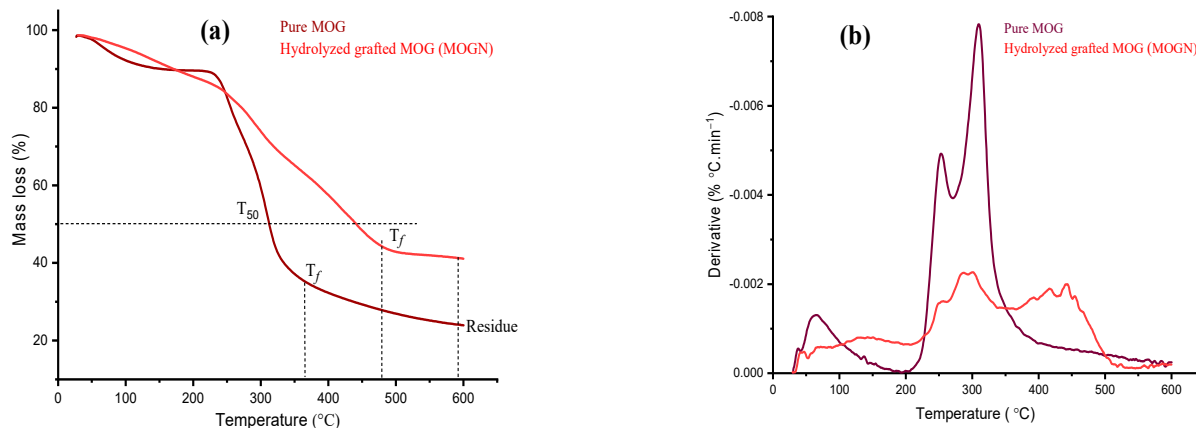


Figure 5. Thermal analysis of the pure MOG and MOGN (a) TGA and (b) DTG curves.

3.3. Swelling Studies of MOGN

Synthesized MOGN behaves as a superabsorbent nanogel as it can hold a huge amount of water in its network with a maximum uptake of 365.0 g/g (Figure 6a,b). Such a high superabsorbent property of water uptake comes from the partial hydrolysis of the $-NH_2$ groups on the polymer skeleton, resulting in the generation of COO^- groups. The ionized $-COOH$ groups thus formed, and the innate carboxylic groups of glucuronic acid in the polymer skeleton of MOG bestowed a huge water-absorbing capacity to MOGN [57]. The equilibrium P_s of 650; 910; 2100; 5370 at pH 2.4, 3.5, 4.5, 5.0 in 1080 min (18 h) and 10,500; 36,300; 9700 and 4250 at pH 5.5, distilled water (6.0), 6.8, 7.4 was attained in 4320 min (72 h) at 37 °C, respectively (Figure 6c,d). From the results, it is revealed that the maximum P_s of MOGN at 37 °C with pH-responsiveness to water uptake was in order: 6.0 > 5.5 > 6.8 > 7.4 > 5.0 > 4.5 > 3.5 > 2.4. Such a trend of swelling of the MOGN can be attributed to its changing behavior with pH. At low pH, the suppression of its ionized carboxylic groups occurs due to the presence of H^+ ions in the external medium. At an alkaline pH, the interactions of the unionized carboxylic groups with water molecules are hindered due to the presence of basic moieties on the surface of nanogel. Thus, the overall effect results in the highest swelling at pH 6.0 [46]. Thus, the water absorption capacity of MOGN is pH-dependent, indicative of its stimuli-responsive swelling nature. These features, viz. high-water adsorption capacity and pH-responsive nature of the synthesized material in the pH range of cancerous cells, 5.0–6.8, are the two important attributes that make it the proficient candidate for the site-specific drug delivery platform to ensure the effective release of DOX.

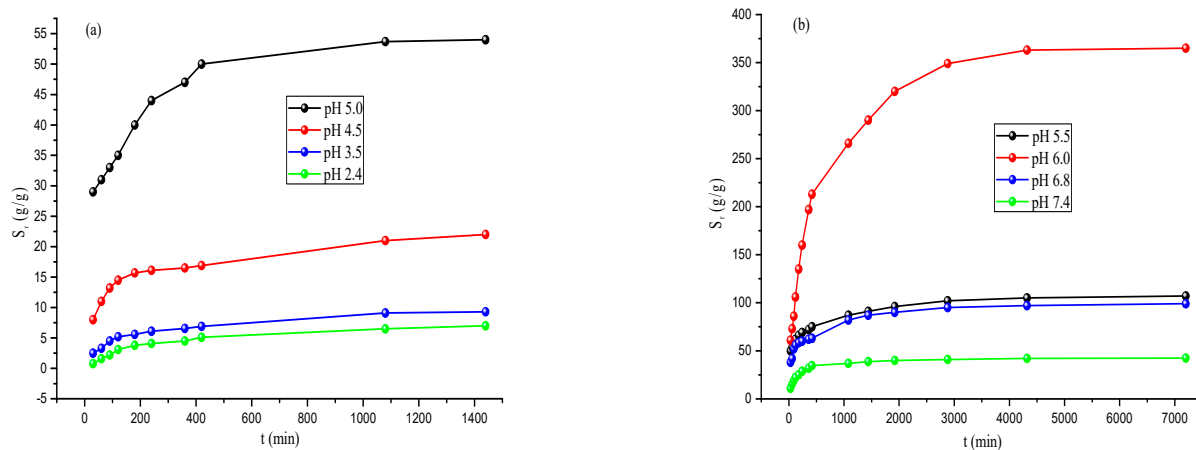


Figure 6. Cont.

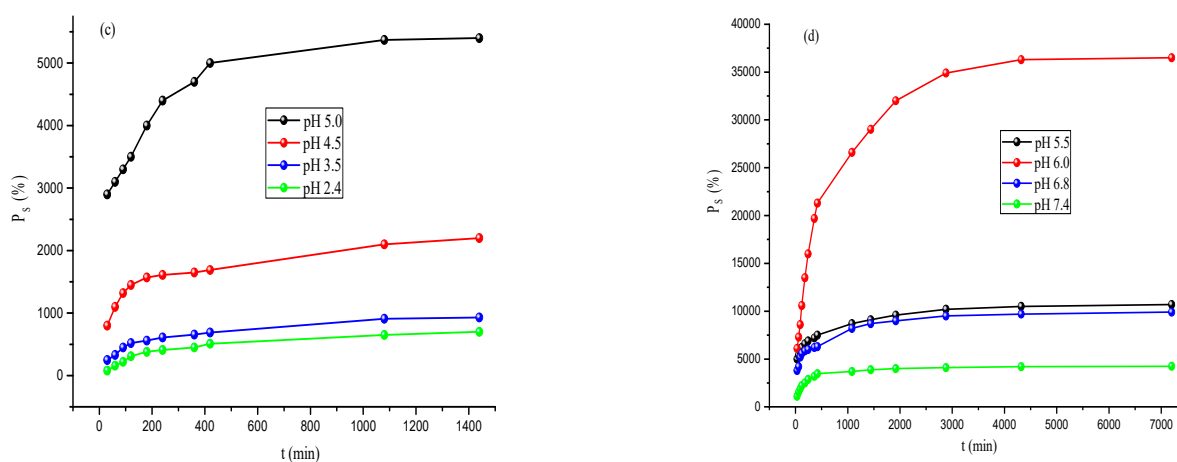
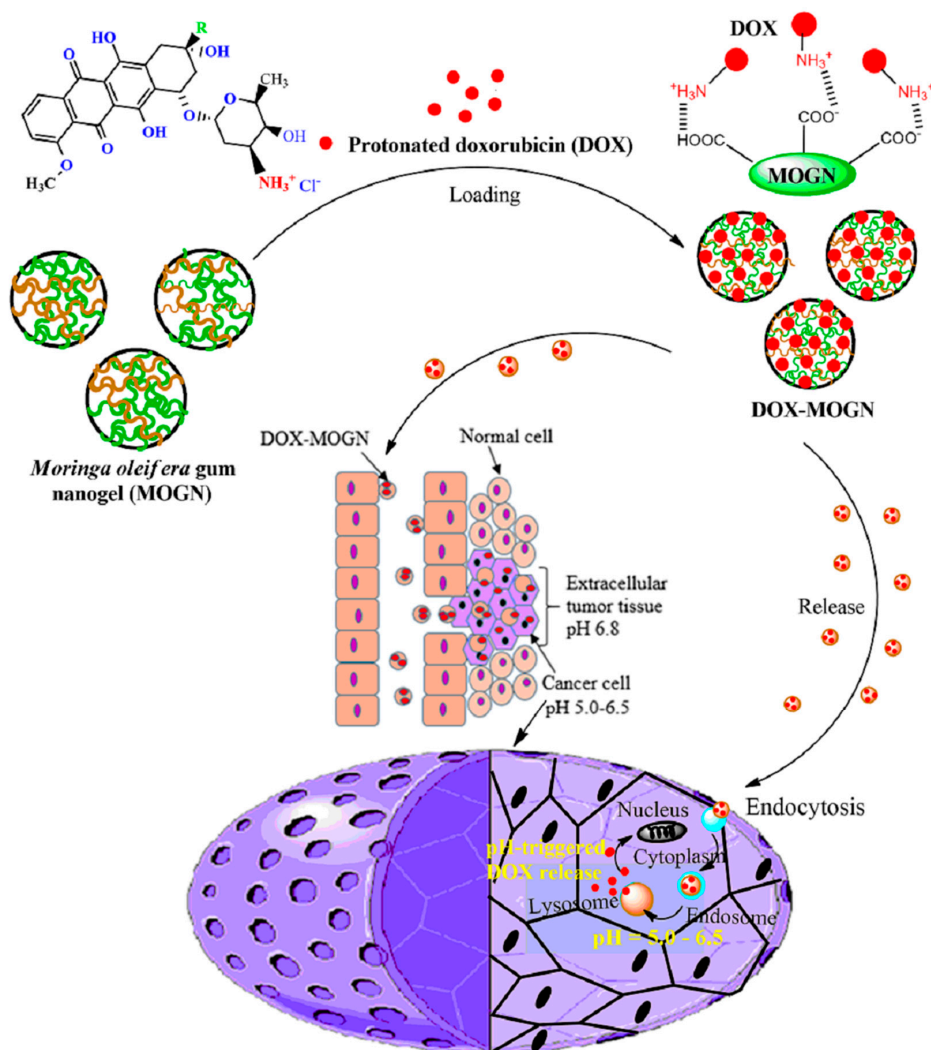


Figure 6. Swelling ratio (S_r) of the MOGN at 37 °C for pHs (2.4–5.0) from 5–1400 min (a) and pHs (5.5–7.4) from 5–7200 min (b); % swelling (P_s) of MOGN at 37 °C for pH (2.4–5.0) from 5–1440 min (c) and pHs (5.5–7.4) from 5–7200 min (d).

3.4. DOX Loading and Release Studies

DOX loading onto MOGN and its release from there have been schematically presented in Scheme 3. This is attributed to the presence of sufficiently available ionized carboxylic groups ($-\text{COO}^-$) present in the MOGN skeleton, which attracts the protonated amino groups ($-\text{NH}_3^+$) of DOX via electrostatic interactions [24,58]. It was observed that DOX-MOGN showed a very high %loading (%L) of 98.35% of DOX on MOGN (Figure 7a). UV-spectral studies further confirmed that the DOX loading onto MOGN was observed from a decrease in the absorbance of the DOX concentration with time (Figure 7b). Pikabea et al. observed a similar trend for loading efficiency for PDEAEMA-based nanogel; however, the synthesized nanogel, MOGN, showed a higher %L than PDEAEMA-based nanogel (90%) and other reported nanogels in the literature elsewhere [22,23,28,30]. Thus, the MOGN fulfills the primary objective of high drug loading for effective dosage for the localized release at the affected part of the body.

To evaluate the pH-triggered DOX release behaviour, *in vitro* release studies of DOX from DOX-MOGN with time was investigated at 37 °C under different pH media of 5.5, 6.8, and 7.4 [16,27]. From the release profile, it was observed that the release of DOX from DOX-MOGN was both time and pH-dependent. About 9.06% in 24 h and 12.18% in 72 h release of DOX from MOGN was observed at pH 7.4. This can be ascribed to the equilibrium partitioning effect between NH_3^+ groups of DOX and COO^- groups of the nanogel. At pH 5.5 and pH 6.8, DOX release was found to be much higher, i.e., 83.42% and 53.72% in 24 h, and 91.92% and 62.62% in 72 h, respectively, due to the combined effect of the weakening of electrostatic interactions between the DOX and nanogel at the acidic pH along with the pH-triggered swelling-cum-disintegration of the MOGN (Figure 8a) [25,58]. Therefore, it can be concluded that the amount of DOX released was maximum at pH 5.5 and least at pH 7.4. This trend is attributed to the combined effect of enhanced swelling at acidic pH, diffusion of the drug, and nanogel disintegration [27]. Since DOX release was maximum at pH 5.5, the stability of this pH-responsive system at pH 7.4 was advantageous as DOX was not released during blood circulation and would lessen the toxic effects associated with the free drug.



Scheme 3. Schematic presentation of the DOX loading and pH-triggered intracellular DOX release from DOX-MOBN in a tumor cell.

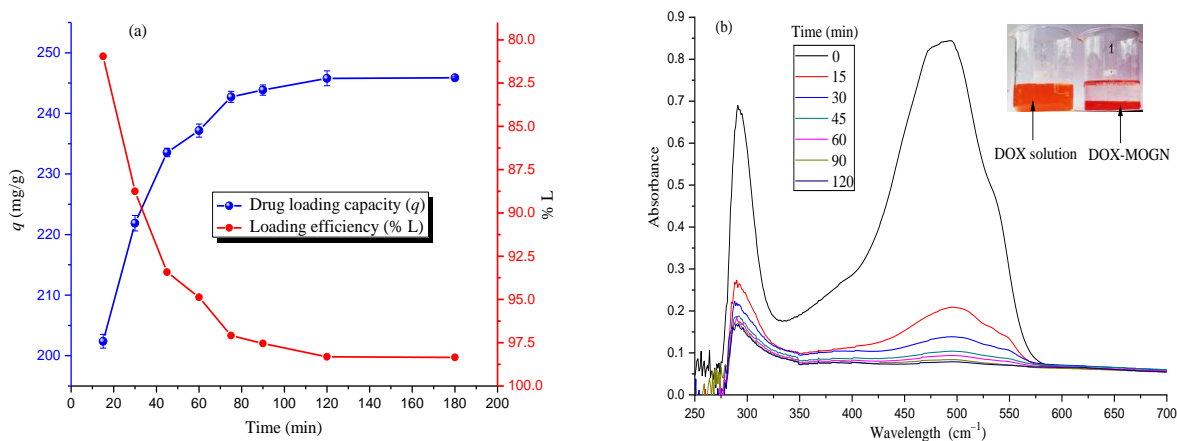


Figure 7. Drug loading capacity (q) and loading efficiency (%L) of DOX onto MOGN at 37 °C with time (a) and UV-spectrum of DOX loading onto MOGN with time (inset image of 250 mg/L DOX solution and DOX-loaded on MOGN) (b).

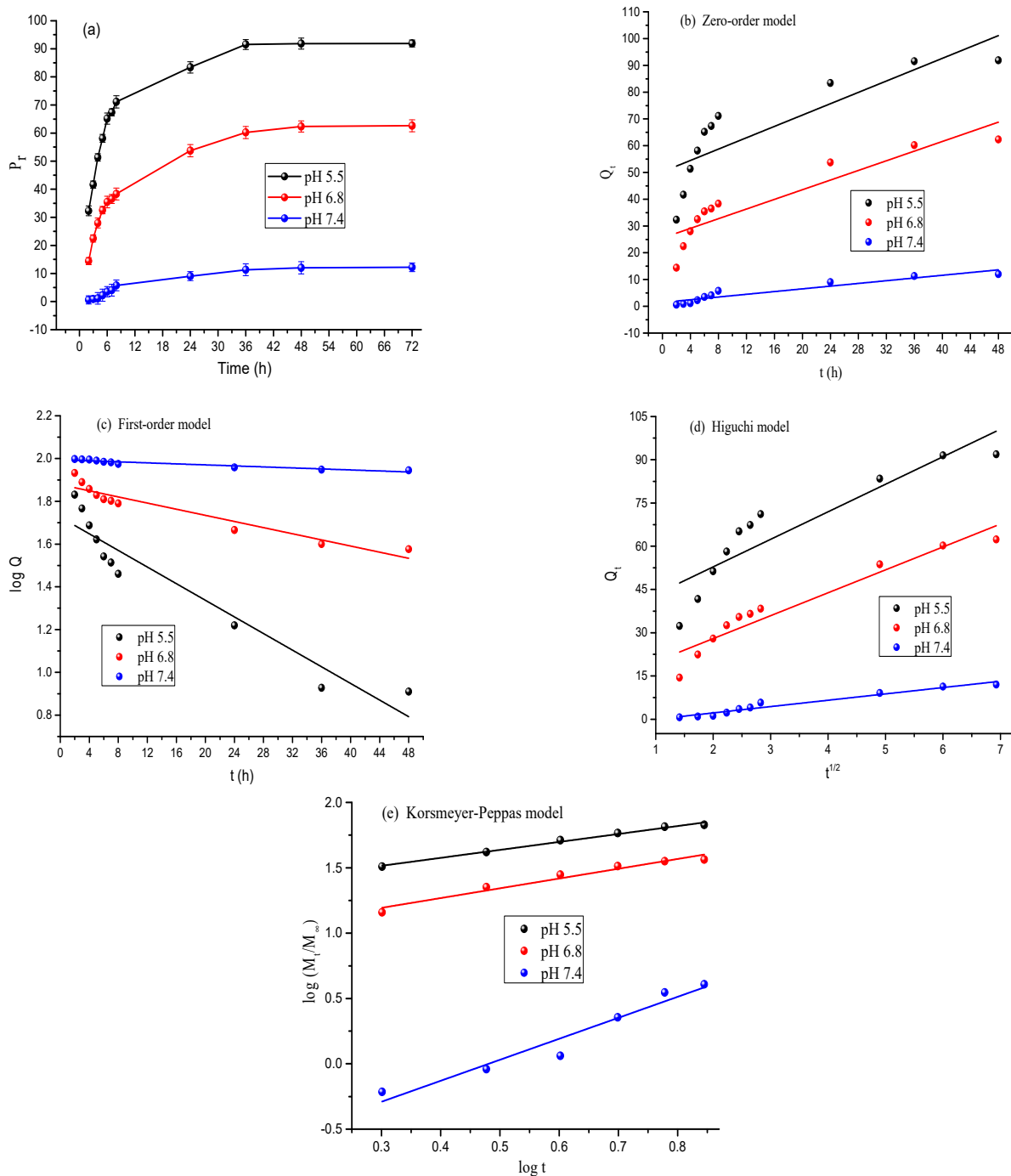


Figure 8. %Release (P_t) of DOX with time (a); drug release kinetic plots for DOX release from the DOX-MOBN under different pH conditions release: (b) zero-order, (c) first-order, (d) Higuchi and (e) Korsmeyer–Peppas plot.

Plots of different drug-release kinetic models are shown in Figure 8b–e. Therefrom, it can be observed that at pH 5.5 and 6.8, the release of DOX from DOX-MOBN followed the Korsmeyer–Peppas release model with the highest value of correlation coefficient, R^2 , 0.99, and 0.952, respectively (Table 2). The best fit of the Korsmeyer–Peppas model indicated the diffusion and the swelling-controlled release of DOX from DOX-MOBN, further validated by the values of n obtained from the slope of the Korsmeyer–Peppas plot. From Table 2, the values of n at pH 5.5 and 6.8 were 0.61 and 0.75, respectively, suggesting an anomalous non-Fickian transport mechanism, meaning that the drug release mechanism

was governed by diffusion and swelling of DOX–MOGN [59,60]. But at pH 7.4, the release of DOX from DOX–MOGN followed the Higuchi kinetic model with the highest R^2 value of 0.956, suggesting a diffusion-controlled release mechanism [61].

Table 2. Release parameters of different kinetic models for DOX at different pHs.

| Kinetic Model | Parameters | pHs | | |
|------------------|------------|-------|-------|-------|
| | | 5.5 | 6.8 | 7.4 |
| Zero-order | R^2 | 0.682 | 0.816 | 0.886 |
| | k_0 | 1.06 | 0.902 | 0.254 |
| First-order | R^2 | 0.907 | 0.897 | 0.895 |
| | k_1 | 0.019 | 0.007 | 0.001 |
| Higuchi | R^2 | 0.808 | 0.916 | 0.956 |
| | k_H | 9.55 | 7.95 | 2.2 |
| Korsmeyer–Peppas | R^2 | 0.99 | 0.952 | 0.933 |
| | k_{KP} | 3.79 | 2.63 | 0.46 |
| | n | 0.61 | 0.75 | 1.61 |

A comparison of %L and P_r of DOX for various nanogels with the synthesized MOGN was presented in Table 3. Therefrom, it was revealed that the synthesized MOGN is an efficient DOX delivery device with a high loading efficiency of 98.35% and P_r of 91.92%, 62.62%, and 12.18% at pH 5.5, 6.8, and 7.4 after 72 h, respectively.

Table 3. Comparison of the loading efficiency (%L) and %release (P_r) of DOX for various drug delivery devices with the synthesized MOGN.

| Drug Delivery Devices | %L | pH | P_r | Time (h) | References |
|--------------------------|------------|-----|------------|----------|------------|
| CMXG@AuNPs | 96.4 ± 0.6 | 5.3 | 98 ± 4.2 | 12 | [4] |
| | | 6.6 | 89 ± 1.8 | | |
| | | 7.4 | 6.67 ± 2.5 | | |
| PEG-CMCS-SS-PDPA | — | 5.0 | >81.32 | 57 | [5] |
| IHC nanoparticles | 79.0 ± 2.1 | 5.0 | 67.8 | 100 | [6] |
| | | 6.5 | 50.2 | | |
| | | 7.4 | 35 | | |
| (Cys-PMO) | 76 | 5.5 | 56 | 48 | [16] |
| | | 7.4 | 10 | | |
| Chitin-PCLCNGs | 80.0 | 6.0 | 45.3 | 72 | [22] |
| | | 7.4 | 36.3 | | |
| <i>n</i> -Dxt-p(MBA)-pAA | 86.0 | 5.5 | 57.0 | 72 | [23] |
| | | 7.4 | 34.0 | | |
| Carboxymethyl-chitosan | 94.7 | 5.0 | 95.1 | 240 | [25] |
| | | 6.5 | 67.2 | | |
| | | 7.4 | 11.7 | | |
| Dextrin | 65–70 | 5.0 | 100 | 72 | [27] |
| | | 6.8 | 94.0 | | |
| | | 7.4 | 40.0 | | |
| Hyaluronate | 63.2 | 5.5 | 86.0 | 72 | [30] |
| | | 6.8 | 60.1 | | |
| | | 7.4 | 38.5 | | |

Table 3. Cont.

| Drug Delivery Devices | %L | pH | P _r | Time (h) | References |
|------------------------------|--------------|-----|----------------|----------|---------------|
| Pullulan | 70.0 | 5.0 | 46.0 | 190 | [31] |
| | | 6.5 | 34.2 | | |
| | | 7.4 | 20.5 | | |
| CTNGs | 9.9 | 5.5 | 70.0 | 12 | [32] |
| | | 7.4 | 35.0 | | |
| Xanthan gum nanogel | — | 5.0 | 72.1 | 72 | [40] |
| | | 6.5 | 55.2 | | |
| | | 7.4 | 38.3 | | |
| PEGylated nanogel | 80.0 | 5.3 | 39.0 | 50 | [62] |
| | | 7.4 | 13.0 | | |
| Chitosan-based nanoparticles | ~75 | 4.5 | >80 | 48 | [63] |
| | | 6.5 | ~70 | | |
| | | 7.4 | ~25 | | |
| GO-Phe-CD nanocomposite | 78.7 | 5.3 | 40 | 72 | [64] |
| | | 7.4 | 12 | | |
| GQDs-PAMAM-β-CD | 61.2 | 5.0 | 73.87 | 96 | [65] |
| | | 7.4 | 24.5 | | |
| Hyaluronic acid nanogels | 83.33 ± 3.21 | 5.5 | 61.4 | 48 | [66] |
| | | 7.4 | 27.2 | | |
| CMC/PCL nanofibers | >90 | 5.5 | ~80 | ~160 | [67] |
| | | 7.4 | ~35 | | |
| HAHG-B hydrogel | 94 | 5.0 | ~68 | 96 | [68] |
| | | 7.4 | ~32 | | |
| DOX-hyd-PEG-FA | — | 5.0 | 94 | 58 | [69] |
| | | 7.4 | 12 | | |
| MOGN | 98.35 | 5.5 | 91.92 | 72 | Present study |
| | | 6.8 | 62.62 | | |
| | | 7.4 | 12.18 | | |

3.5. In Vitro Cytotoxicity Studies

The cytotoxicity of the DOX delivery platform was investigated and compared with the free DOX using RD cells. Normal RD cells had a spindle shape, but after treatment with free-DOX and DOX-MOBN, the cell shape got distorted as the dead cells assumed a spherical shape (Figure 9a–c). The cytotoxicity of DOX-MOBN was concentration-dependent, and cell viability of 7.0% at pH 5.5 was observed for DOX-MOBN (Figure 9d) [70]. Moreover, IC₅₀ of RD cells treated with DOX-MOBN (0.946 µg/mL) at pH 5.5 was near to the IC₅₀ of free DOX (0.812 µg/mL), confirming the maximum release of DOX from MOBN at pH 5.5 [16]. Thus, in vitro cytotoxicity studies displayed close consonance with in vitro release studies. Hence, the effective release at intracellular pH 5.5 makes MOBN an excellent DOX nanocarrier for its pH-triggered release at the cancer site.

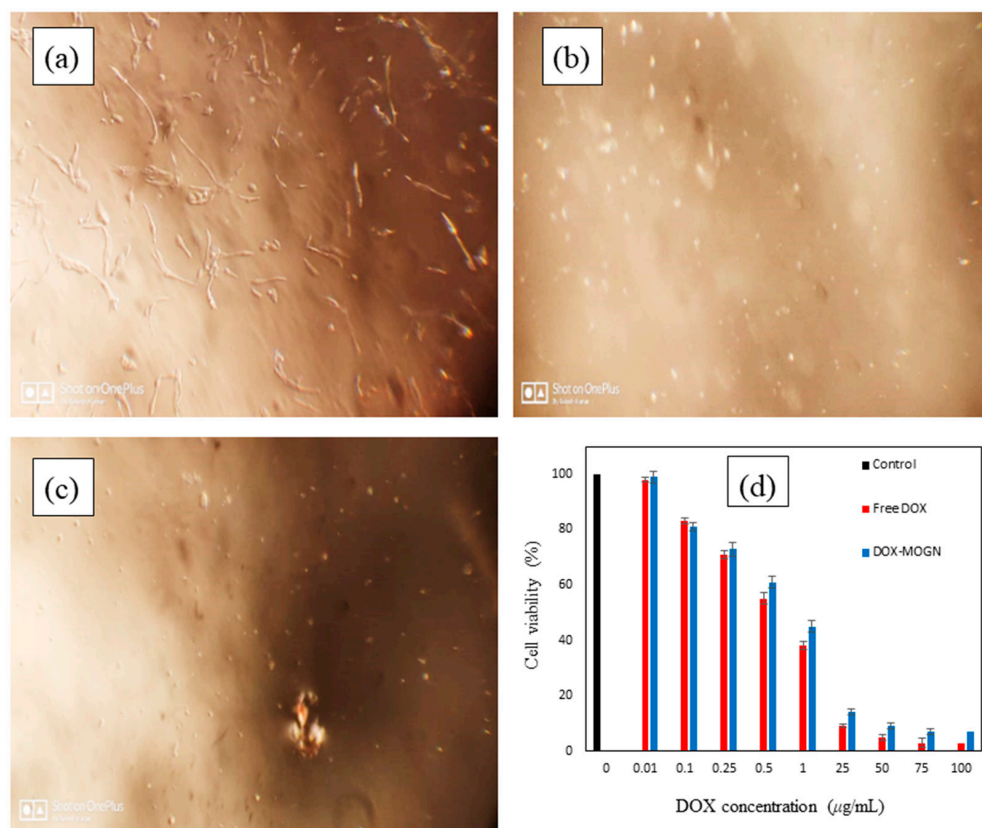


Figure 9. Images of the control (untreated RD cells) (a), free DOX treated RD cells (b), DOX–MOBN treated RD cells (c); in vitro cell viability of RD cells treated with different DOX concentrations (d).

4. Conclusions

In the present research work, *M. oleifera* gum nanogel, MOBN, was successfully synthesized via γ -irradiation, followed by partial hydrolysis, sonication, and ultracentrifugation. Thereafter, MOBN was evaluated as a nanocarrier for DOX delivery. MOBN showed a high swelling ratio within the pH range of cancerous cells, i.e., 5.0–6.8, with a maximum swelling ratio of 365.0 g/g at pH 6.0 and 37 °C. MOBN exhibited a very high %L (98.35%) of DOX. The release kinetics of DOX from DOX–MOBN at pH 5.5 and 6.8 follows the Korsmeyer–Peppas model, whereas at pH 7.4, it follows the Higuchi kinetic model. The DOX release from DOX–MOBN was the highest at simulated endosomal and extracellular pH of the tumor tissue, i.e., pH 5.5 (91.92%) and the lowest at pH 7.4 (12.18%), thereby indicating that DOX–MOBN can deliver DOX specifically to the tumor cells. In addition, the optimal DOX release and cytotoxicity studies at pH 5.5 are in consonance. The results obtained suggest that the pH-responsive *M. oleifera* nanogel is an effective intracellular drug delivery system for DOX cancer therapy and is capable of reducing the side effects of anticancer drugs.

Author Contributions: Conceptualization, G.S.C., S.R. and V.J.; methodology, G.S.C. and S.R.; software, S.R., S.C. and K.K.; validation, S.R. and G.S.C.; formal analysis, S.R.; investigation, S.R. and R.K.; resources, S.R., S.C. and K.K.; data curation, S.R. and R.K.; writing—original draft preparation, S.R. and M.K.; writing—review and editing, G.S.C., S.R., M.K. and M.M.; visualization, S.R. and M.M.; supervision, G.S.C. and V.J. All authors have read and agreed to the published version of the manuscript.

Funding: This research is partially supported by the European Union’s Horizon 2020 research and Innovation Programme under the Marie Skłodowska-Curie grant agreement No 847639 and from the Ministry of Education and Science.

Institutional Review Board Statement: Not applicable.

Informed Consent Statement: Not applicable.

Data Availability Statement: Not applicable.

Acknowledgments: The authors acknowledge the facilities provided by the Department of Chemistry and Department of Biotechnology, Himachal Pradesh University, India, to carry out this work. The authors also acknowledge Judit E. Puskas, Department of Food, Agriculture and Biological Engineering, The Ohio State University, United States, for valuable discussion.

Conflicts of Interest: The authors declare no conflict of interest.

References

1. Wild, C.P.; Weiderpass, E.; Stewart, B.W. *World Cancer Report: Cancer Research for Cancer Prevention*; International Agency for Research on Cancer: Lyon, France, 2020. Available online: <https://publications.iarc.fr/586> (accessed on 4 February 2020).
2. Ferlay, J.; Colombet, M.; Soerjomataram, I.; Mathers, C.; Parkin, D.M.; Piñeros, M.; Znaor, A.; Bray, F. Estimating the Global Cancer Incidence and Mortality in 2018: GLOBOCAN Sources and Methods. *Int. J. Cancer* **2018**, *144*, 1941–1953. [[CrossRef](#)] [[PubMed](#)]
3. Sung, H.; Ferlay, J.; Siegel, R.L.; Laversanne, M.; Soerjomataram, I.; Jemal, A.; Bray, F. Global Cancer Statistics 2020: GLOBOCAN Estimates of Incidence and Mortality Worldwide for 36 Cancers in 185 Countries. *CA Cancer J. Clin.* **2021**, *71*, 209–249. [[CrossRef](#)] [[PubMed](#)]
4. Alle, M.; Kim, T.H.; Park, S.H.; Lee, S.-H.; Kim, J.-C. Doxorubicin-Carboxymethyl Xanthan Gum Capped Gold Nanoparticles: Microwave Synthesis, Characterization, and Anti-Cancer Activity. *Carbohydr. Polym.* **2020**, *229*, 115511. [[CrossRef](#)] [[PubMed](#)]
5. Xie, P.; Liu, P. pH-Responsive Surface Charge Reversal Carboxymethyl Chitosan-Based Drug Delivery System for pH and Reduction Dual-Responsive Triggered DOX Release. *Carbohydr. Polym.* **2020**, *236*, 116093. [[CrossRef](#)] [[PubMed](#)]
6. Xu, Z.; Yang, D.; Long, T.; Yuan, L.; Qiu, S.; Li, D.; Mu, C.; Ge, L. pH-Sensitive Nanoparticles Based on Amphiphilic Imidazole/Cholesterol Modified Hydroxyethyl Starch for Tumor Chemotherapy. *Carbohydr. Polym.* **2022**, *277*, 118827. [[CrossRef](#)] [[PubMed](#)]
7. Xie, P.; Liu, P. Core-Shell-Corona Chitosan-Based Micelles for Tumor Intracellular pH-Triggered Drug Delivery: Improving Performance by Grafting Polycation. *Int. J. Biol. Macromol.* **2019**, *141*, 161–170. [[CrossRef](#)]
8. Zhang, Y.; Song, W.; Lu, Y.; Xu, Y.; Wang, C.; Yu, D.-G.; Kim, I. Recent Advances in Poly(α -L-glutamic acid)-Based Nanomaterial for Drug Delivery. *Biomolecules* **2022**, *12*, 636. [[CrossRef](#)]
9. Liao, J.; Zheng, H.; Fei, Z.; Lu, B.; Zheng, H.; Li, D.; Xiong, X.; Yi, Y. Tumor-Targeting and pH-Responsive Nanoparticles from Hyaluronic Acid for the Enhanced Delivery of Doxorubicin. *Int. J. Biol. Macromol.* **2018**, *113*, 737–747. [[CrossRef](#)]
10. Liu, P.; Chen, N.; Yan, L.; Gao, F.; Ji, D.; Zhang, S.; Zhang, L.; Li, Y.; Xiao, Y. Preparation, Characterisation and In Vitro and In Vivo Evaluation of CD44-Targeted Chondroitin Sulphate-Conjugated Doxorubicin PLGA Nanoparticles. *Carbohydr. Polym.* **2019**, *213*, 17–26. [[CrossRef](#)]
11. Tolle, C.; Riedel, J.; Mikolai, C.; Winkel, A.; Stiesch, D.W.; Menzel, H. Biocompatible Coatings from Smart Biopolymer Nanoparticles for Enzymatically Induced Drug Release. *Biomolecules* **2018**, *s8*, 103. [[CrossRef](#)]
12. Prabaharan, M. Chitosan-Based Nanoparticles for Tumor-Targeted Drug Delivery. *Int. J. Biol. Macromol.* **2015**, *72*, 1313–1322. [[CrossRef](#)] [[PubMed](#)]
13. Elbially, N.S.; Fathy, M.M.; Khalil, W.M. Doxorubicin Loaded Magnetic Gold Nanoparticles for In Vivo Targeted Drug Delivery. *Int. J. Pharm.* **2015**, *490*, 190–199. [[CrossRef](#)] [[PubMed](#)]
14. Wang, F.; Wang, Y.-C.; Dou, S.; Xiong, M.-H.; Sun, T.-M.; Wang, J. Doxorubicin-Tethered Responsive Gold Nanoparticles Facilitate Intracellular Drug Delivery for Overcoming Multidrug Resistance in Cancer Cells. *ACS Nano* **2011**, *5*, 3679–3692. [[CrossRef](#)] [[PubMed](#)]
15. van Elk, M.; Deckers, R.; Oerlemans, C.; Shi, Y.; Storm, G.; Vermonden, T.; Hennink, W.E. Triggered Release of Doxorubicin from Temperature-Sensitive Poly (N-(2-Hydroxypropyl)-Methacrylamide Mono/Dilactate) Grafted Liposomes. *Biomacromolecules* **2014**, *15*, 1002–1009. [[CrossRef](#)]
16. Rao, K.M.; Parambadath, S.; Kumar, A.; Ha, C.-S.; Han, S.S. Tunable Intracellular Degradable Periodic Mesoporous Organosilica Hybrid Nanoparticles for Doxorubicin Drug Delivery in Cancer Cells. *ACS Biomater. Sci. Eng.* **2018**, *4*, 175–183. [[CrossRef](#)] [[PubMed](#)]
17. Zhang, Q.; Liu, F.; Nguyen, K.T.; Ma, X.; Wang, X.; Xing, B.; Zhao, Y. Multifunctional Mesoporous Silica Nanoparticles for Cancer-Targeted and Controlled Drug Delivery. *Adv. Funct. Mater.* **2012**, *22*, 5144–5156. [[CrossRef](#)]
18. Du, Y.; Chen, W.; Zheng, M.; Meng, F.; Zhong, Z. pH-Sensitive Degradable Chimaeric Polymersomes for the Intracellular Release of Doxorubicin Hydrochloride. *Biomaterials* **2012**, *33*, 7291–7299. [[CrossRef](#)]
19. Shafiee, S.; Ahangar, H.A.; Saffar, A. Taguchi Method Optimization for Synthesis of Fe₃O₄@Chitosan/Tragacanth Gum Nanocomposite as a Drug Delivery System. *Carbohydr. Polym.* **2019**, *222*, 114982. [[CrossRef](#)] [[PubMed](#)]
20. Chen, C.-K.; Wang, Q.; Jones, C.H.; Yu, Y.; Zhang, H.; Law, W.-C.; Lai, C.K.; Zeng, Q.; Prasad, P.N.; Pfeifer, B.A. Synthesis of pH-Responsive Chitosan Nanocapsules for the Controlled Delivery of Doxorubicin. *Langmuir* **2014**, *30*, 4111–4119. [[CrossRef](#)]

21. Hoelzer, D.; Leiske, M.N.; Hartlieb, M.; Bus, T.; Pretzel, D.; Hoepfner, S.; Kempe, K.; Thierbach, R.; Schubert, U.S. Tumor Targeting with pH-Responsive Poly (2-Oxazoline)-Based Nanogels for Metronomic Doxorubicin Treatment. *Oncotarget* **2018**, *9*, 22316–22331. [[CrossRef](#)]
22. Arunraj, T.R.; Rejinold, N.S.; Kumar, N.A.; Jayakumar, R. Doxorubicin-Chitin-Poly (Caprolactone) Composite Nanogel for Drug Delivery. *Int. J. Biol. Macromol.* **2013**, *62*, 35–43. [[CrossRef](#)] [[PubMed](#)]
23. Das, D.; Rameshbabu, A.P.; Ghosh, P.; Patra, P.; Dhara, S.; Pal, S. Biocompatible Nanogel Derived from Functionalized Dextrin for Targeted Delivery of Doxorubicin Hydrochloride to MG 63 Cancer Cells. *Carbohydr. Polym.* **2017**, *171*, 27–38. [[CrossRef](#)] [[PubMed](#)]
24. He, L.; Liang, H.; Lin, L.; Shah, B.R.; Li, Y.; Chen, Y.; Li, B. Green-Step Assembly of Low Density Lipoprotein/Sodium Carboxymethyl Cellulose Nanogels for Facile Loading and pH-Dependent Release of Doxorubicin. *Colloids Surf. B Biointerfaces* **2015**, *126*, 288–296. [[CrossRef](#)] [[PubMed](#)]
25. Li, S.; Hu, L.; Li, D.; Wang, X.; Zhang, P.; Wang, J.; Yan, G.; Tang, R. Carboxymethyl Chitosan-Based Nanogels via Acid-Labile Ortho Ester Linkages Mediated Enhanced Drug Delivery. *Int. J. Biol. Macromol.* **2019**, *129*, 477–487. [[CrossRef](#)]
26. Jayakumar, R.; Nair, A.; Rejinold, N.S.; Maya, S.; Nair, S.V. Doxorubicin-Loaded pH-Responsive Chitin Nanogels for Drug Delivery to Cancer Cells. *Carbohydr. Polym.* **2012**, *87*, 2352–2356. [[CrossRef](#)]
27. Manchun, S.; Cheewatanakornkool, K.; Dass, C.R.; Sriamornsak, P. Novel pH-Responsive Dextrin Nanogels for Doxorubicin Delivery to Cancer Cells with Reduced Cytotoxicity to Cardiomyocytes and Stem Cells. *Carbohydr. Polym.* **2014**, *114*, 78–86. [[CrossRef](#)]
28. Pikabea, A.; Villar-Alvarez, E.; Forcada, J.; Taboada, P. pH-Controlled Doxorubicin Delivery from PDEAEMA-Based Nanogels. *J. Mol. Liq.* **2018**, *66*, 321–329. [[CrossRef](#)]
29. Sun, Z.; Yi, Z.; Zhang, H.; Ma, X.; Su, W.; Sun, X.; Li, X. Bio-responsive Alginate-Keratin Composite Nanogels with Enhanced Drug Loading Efficiency for Cancer Therapy. *Carbohydr. Polym.* **2017**, *175*, 159–169. [[CrossRef](#)] [[PubMed](#)]
30. Zhang, Y.; Wang, F.; Li, M.; Yu, Z.; Qi, R.; Ding, J.; Zhang, Z.; Chen, X. Self-Stabilized Hyaluronate Nanogel for Intracellular Codelivery of Doxorubicin and Cisplatin to Osteosarcoma. *Adv. Sci.* **2018**, *5*, 1700821. [[CrossRef](#)]
31. Zheng, Y.; Lv, X.; Xu, Y.; Cheng, X.; Wang, X.; Tang, R. pH-Sensitive and Pluronic-Modified Pullulan Nanogels for Greatly Improved Antitumor In Vivo. *Int. J. Biol. Macromol.* **2019**, *139*, 277–289. [[CrossRef](#)] [[PubMed](#)]
32. Zuo, Y.; Kong, M.; Mu, Y.; Feng, C.; Chen, X. Chitosan Based Nanogels Stepwise Response to Intracellular Delivery Kinetics for Enhanced Delivery of Doxorubicin. *Int. J. Biol. Macromol.* **2017**, *104*, 157–164. [[CrossRef](#)] [[PubMed](#)]
33. Mura, S.; Nicolas, J.; Couvreur, P. Stimuli-Responsive Nanocarriers for Drug Delivery. *Nat. Mater.* **2013**, *12*, 991–1003. [[CrossRef](#)] [[PubMed](#)]
34. Dispenza, C.; Giacomazza, D.; Jonsson, M. Micro- to Nanoscale Bio-Hybrid Hydrogels Engineered by Ionizing Radiation. *Biomolecules* **2021**, *11*, 47. [[CrossRef](#)] [[PubMed](#)]
35. Arjama, M.; Mehnath, S.; Rajan, M.; Jeyaraj, M. Sericin/RBA Embedded Gellan Gum Based Smart Nanosystem for pH Responsive Drug Delivery. *Int. J. Biol. Macromol.* **2018**, *120*, 1561–1571. [[CrossRef](#)] [[PubMed](#)]
36. Barclay, T.G.; Day, C.M.; Petrovsky, N.; Garg, S. Review of Polysaccharide Particle-Based Functional Drug Delivery. *Carbohydr. Polym.* **2019**, *22*, 94–112. [[CrossRef](#)] [[PubMed](#)]
37. Debele, T.A.; Mekuria, S.L.; Tsai, H.-C. Polysaccharide Based Nanogels in the Drug Delivery System: Application as the Carrier of Pharmaceutical Agents. *Mater. Sci. Eng. C* **2016**, *68*, 964–981. [[CrossRef](#)] [[PubMed](#)]
38. Chauhan, G.S. Evaluation of Nanogels as Supports for Enzyme Immobilization. *Polym. Int.* **2014**, *63*, 1889–1894. [[CrossRef](#)]
39. Yu, J.; Zhang, Y.; Sun, W.; Wang, C.; Ranson, D.; Ye, Y.; Weng, Y.; Gu, Z. Internalized Compartments Encapsulated Nanogels for Targeted Drug Delivery. *Nanoscale* **2016**, *8*, 9178–9184. [[CrossRef](#)]
40. Zhang, L.; Xu, J.; Wen, Q.; Ni, C. Preparation of Xanthan Gum Nanogels and Their pH/Redox Responsiveness in Controlled Release. *J. Appl. Polym. Sci.* **2019**, *136*, 47921. [[CrossRef](#)]
41. Wasti, A.T.; Mandeville, H.; Gatz, S.; Chisholm, J.C. Rhabdomyosarcoma. *Paediatr. Child Health* **2018**, *28*, 157–163. [[CrossRef](#)]
42. Werner, M.; Atil, B.; Sieczkowski, E.; Chiba, P.; Hohenegger, M. Simvastatin-induced compartmentalisation of doxorubicin sharpens up nuclear topoisomerase II inhibition in human rhabdomyosarcoma cells. *Naunyn-Schmiedeberg's Arch. Pharmacol.* **2013**, *386*, 605–617. [[CrossRef](#)] [[PubMed](#)]
43. Ranote, S.; Ram, B.; Kumar, D.; Chauhan, G.S.; Joshi, V. Functionalization of *Moringa oleifera* Gum for use as Hg²⁺ Ions Adsorbent. *J. Environ. Chem. Eng.* **2018**, *6*, 1805–1813. [[CrossRef](#)]
44. Francis, S.; Mitra, D.; Dhanawade, B.R.; Varshney, L.; Sabharwal, S. Gamma Radiation Synthesis of Rapid Swelling Superporous Polyacrylamide Hydrogels. *Radiat. Phys. Chem.* **2009**, *78*, 951–953. [[CrossRef](#)]
45. Toti, U.S.; Aminabhavi, T.M. Modified Guar Gum Matrix Tablet for Controlled Release of Diltiazem Hydrochloride. *J. Control. Release* **2004**, *95*, 567–577. [[CrossRef](#)] [[PubMed](#)]
46. Chauhan, G.S.; Chauhan, S. Synthesis, Characterization, and Swelling Studies of pH- and Thermosensitive Hydrogels for Specialty Applications. *J. Appl. Polym. Sci.* **2008**, *109*, 47–55. [[CrossRef](#)]
47. Bruschi, M.L. Mathematical Models of Drug Release. In *Book Strategies to Modify the Drug Release from Pharmaceutical Systems*; Woodhead Publishing: Shaston, UK, 2015; Volume 2, pp. 63–86. ISBN 978-0-08-100092.
48. Dash, S.; Murthy, P.N.; Nath, L.; Chowdhury, P. Kinetic Modeling on Drug Release from Controlled Drug Delivery Systems. *Acta Pol. Pharm.* **2010**, *67*, 217–223.

49. Wagner, J.G. Interpretation of Percent Dissolved-Time Plots Derived from In Vitro Testing of Conventional Tablets and Capsules. *J. Pharm. Sci.* **1969**, *58*, 1253–1257. [[CrossRef](#)]
50. Higuchi, T. Mechanism of Sustained-Action Medication. Theoretical Analysis of Rate of Release of Solid Drugs Dispersed in Solid Matrices. *J. Pharm. Sci.* **1963**, *52*, 1145–1149. [[CrossRef](#)]
51. Korsmeyer, R.W.; Peppas, N.A. Macromolecular and Modeling Aspects of Swelling–Controlled Systems in Controlled Release Delivery Systems. In *Controlled Release Delivery Systems*; Roseman, T.J., Mansdorf, S.Z., Eds.; Marcel Dekker: New York, NY, USA, 1983; pp. 77–90.
52. Hu, H.; Li, Y.; Zhou, Q.; Ao, Y.; Yu, C.; Wan, Y.; Xu, H.; Li, Z.; Yang, X. Redox-Sensitive Hydroxyethyl Starch–Doxorubicin Conjugate for Tumor Targeted Drug Delivery. *ACS Appl. Mater. Interfaces* **2016**, *16*, 30833–30844. [[CrossRef](#)]
53. Liu, J.; Ma, X.; Jin, S.; Xue, X.; Zhang, C.; Wei, T.; Guo, W.; Liang, X.-J. Zinc Oxide Nanoparticles as Adjuvant to Facilitate Doxorubicin Intracellular Accumulation and Visualize pH-Responsive Release for Overcoming Drug Resistance. *Mol. Pharmaceutics* **2016**, *13*, 1723–1730. [[CrossRef](#)]
54. Ranote, S.; Chauhan, G.S.; Joshi, V. Etherified *Moringa oleifera* Gum as Rapid and Effective Dye Adsorbents. *Chem. Eng. J.* **2020**, *387*, 124056. [[CrossRef](#)]
55. Ranote, S.; Kumar, D.; Kumari, S.; Kumar, R.; Chauhan, G.S.; Joshi, V. Green Synthesis of *Moringa oleifera* Gum-Based Bifunctional Polyurethane Foam Braced with Ash for Rapid and Efficient Dye Removal. *Chem. Eng. J.* **2019**, *361*, 1586–1596. [[CrossRef](#)]
56. Hemvichian, K.; Chanthawong, A.; Suwanmala, P. Synthesis and Characterization of Superabsorbent Polymer Prepared by Radiation-Induced Graft Copolymerization of Acrylamide onto Carboxymethyl Cellulose for Controlled Release of Agrochemicals. *Radiat. Phys. Chem.* **2014**, *103*, 167–171. [[CrossRef](#)]
57. Zhang, X.; Wang, X.; Li, L.; Wu, R.; Zhang, S.; Wu, J.; Wu, W. A Novel Polyacrylamide-Based Superabsorbent with Temperature Switch for Steam Breakthrough Blockage. *J. Appl. Polym. Sci.* **2015**, *132*, 42067. [[CrossRef](#)]
58. Li, Y.-M.; Jiang, T.; Lv, Y.; Wu, Y.; He, F.; Zhuo, R.-X. Amphiphilic Copolymers with Pendent Carboxyl Groups for High-Efficiency Loading and Controlled Release of Doxorubicin. *Colloids Surf. B Biointerfaces* **2015**, *132*, 54–61. [[CrossRef](#)] [[PubMed](#)]
59. Jose, S.; Fanguero, J.F.; Smitha, J.; Cinu, T.A.; Chacko, A.J.; Premaletha, K.; Souto, E.B. Predictive Modeling of Insulin Release Profile from Cross-Linked Chitosan Microspheres. *Eur. J. Med. Chem.* **2013**, *60*, 249–253. [[CrossRef](#)] [[PubMed](#)]
60. Mukhopadhyay, P.; Chakraborty, S.; Bhattacharya, S.; Mishra, R.; Kundu, P.P. pH-Sensitive Chitosan/Alginate Core-Shell Nanoparticles for Efficient and Safe Oral Insulin Delivery. *Int. J. Biol. Macromol.* **2015**, *72*, 640–648. [[CrossRef](#)]
61. Kumari, S.; Ram, B.; Kumar, D.; Ranote, S.; Chauhan, G.S. Nanoparticles of Oxidized-Cellulose Synthesized by Green Method. *Mater. Sci. Energy Technol.* **2018**, *1*, 22–28. [[CrossRef](#)]
62. Oishi, M.; Hayashi, H.; Iijima, M.; Nagasaki, Y. Endosomal Release and Intracellular Delivery of Anticancer Drugs Using pH-Sensitive Pegylated Nanogels. *J. Mater. Chem.* **2007**, *17*, 3720–3725. [[CrossRef](#)]
63. Soares, P.I.; Sousa, A.I.; Silva, J.C.; Ferreira, I.M.; Novo, C.M.; Borges, J.P. Chitosan-Based Nanoparticles as Drug Delivery Systems for Doxorubicin: Optimization and Modelling. *Carbohydr. Polym.* **2016**, *147*, 34–312. [[CrossRef](#)]
64. Borandeh, S.; Abdolmaleki, A.; Abolmaali, S.S.; Tamaddon, A.M. Synthesis, Structural and In-Vitro Characterization of B-Cyclodextrin Grafted L-Phenylalanine Functionalized Graphene Oxide Nanocomposite: A Versatile Nanocarrier for pH-Sensitive Doxorubicin Delivery. *Carbohydr. Polym.* **2018**, *201*, 151–161. [[CrossRef](#)] [[PubMed](#)]
65. Pooresmaeil, M.; Namazi, H.; Salehi, R. Synthesis of Photoluminescent Glycodendrimer with Terminal B-Cyclodextrin Molecules as a Biocompatible pH-Sensitive Carrier for Doxorubicin Delivery. *Carbohydr. Polym.* **2020**, *246*, 116658. [[CrossRef](#)] [[PubMed](#)]
66. Zhang, M.; Asghar, S.; Tian, C.; Hu, Z.; Ping, Q.; Chen, Z.; Shao, F.; Xiao, Y. Lactoferrin/Phenylboronic Acid-Functionalized Hyaluronic Acid Nanogels Loading Doxorubicin Hydrochloride for Targeting Glioma. *Carbohydr. Polym.* **2021**, *253*, 117194. [[CrossRef](#)] [[PubMed](#)]
67. Abasalta, M.; Asefnejad, A.; Khorasani, M.T.; Saadatabadi, A.R. Fabrication of Carboxymethyl Chitosan/Poly(ϵ -Caprolactone)/Doxorubicin/Nickel Ferrite Core-Shell Fibers for Controlled Release of Doxorubicin Against Breast Cancer. *Carbohydr. Polym.* **2021**, *257*, 117631. [[CrossRef](#)] [[PubMed](#)]
68. Jo, Y.-J.; Gulfam, M.; Jo, S.-H.; Gal, Y.-S.; Oh, C.-W.; Park, S.-H.; Lim, K.T. Multi-Stimuli Responsive Hydrogels Derived from Hyaluronic Acid for Cancer Therapy Application. *Carbohydr. Polym.* **2022**, *286*, 119303. [[CrossRef](#)]
69. Ye, W.-L.; Du, J.-B.; Zhang, B.-L.; Na, R.; Song, Y.-F.; Mei, Q.-B.; Zhao, M.-G.; Zhou, S.-Y. Cellular Uptake and Antitumor Activity of DOX-hyd-PEGFA Nanoparticles. *PLoS ONE* **2014**, *9*, e97358.
70. Cai, X.; Luo, Y.; Zhang, W.; Du, D.; Lin, Y. pH-Sensitive ZnO Quantum Dots–Doxorubicin Nanoparticles for Lung Cancer Targeted Drug Delivery. *ACS Appl. Mater. Interfaces* **2017**, *9*, 16793–16802.